# Nucleon-nucleon interaction from meson exchange and nucleonic structure

D. Plümper, J. Flender, and M. F. Gari
*Institut für Theoretische Physik, Ruhr-Universität Bochum, 44780 Bochum, Germany*
(Received 26 May 1993; revised manuscript received 21 December 1993)

We discuss the physics of the Bochum $NN$ potential (Ruhrpot). In contrast to conventional one-boson-exchange models (OBE) we calculate the potential within two phases which are (i) meson exchanges at long distances and (ii) direct $NN$ interactions, coming from the intrinsic nucleon structure, at short distances. The interaction vertices are calculated in a self-consistent way. The most important resonant two- and three-$\pi$ correlations are included. As the meson exchange is negligible at high $Q^2$ we have several advantages: (i) reasonable meson scales, (ii) SU(6) limit for vector mesons, (iii) perturbative QCD asymptotic, (iv) no need for $\sigma$ mesons, and (v) very good description of the nucleon-nucleon data.

PACS number(s): 12.39.Pn, 13.75.Cs, 21.30.+y

## I. INTRODUCTION

The nucleon-nucleon interaction plays a very important role in hadron physics. It has been investigated for more than 20 years within a number of different models [1–5], all of which have been partially successful. However, in all of these models there are several inconsistencies with the present understanding of the hadronic structure. External interactions with nuclei demonstrate that the nucleon has a complicated structure, including baryonic and mesonic degrees of freedom. Therefore, in any realistic description of the two nucleon system, such as that obtained from meson-exchange models, the extended structure of the meson-baryon vertex requires the bare vertex to be dressed with vertex corrections, the so-called form factors. It is necessary to determine the vertex corrections within the meson model to be consistent with the potential itself.

In existing boson-exchange models it is found that, in the monopole form, meson scales of more than 1.2 GeV ($NN\pi$) and 1.8 GeV ($NN\rho$) are needed to obtain a reasonable fit to the two nucleon data. By contrast, modern nucleon structure calculations based on Skyrme models [6], nontopological soliton models [7], or bag models [9] obtain much lower meson scales of 0.5 GeV to 0.8 GeV. In an analysis of the $NN\pi$ vertex using several sources, one [8] obtains scales of 0.5 to 0.8 GeV for the free nucleon. Modeling the electromagnetic form factor with pure vector meson dominance and a dipole fit leads to a scale of 0.8 GeV for the $NN\rho$ and the $NN\omega$ vertex. The apparent overestimation of the meson scales used in $NN$ interaction models cannot be resolved by medium effects because modern calculations of the nucleon structure predict a swelling of the nucleon in nuclear matter, which would suggest the scales of 0.5 to 0.8 GeV should be decreased in the $NN$ interaction [10]. Thus the form factors that are used in conventional potential models have to be regarded as pure cutoffs and not as a parametrization of the extended structure of the meson-baryon interaction. Indeed they appear to be artifacts of the potential models and the only processes which are taken into account in a one-boson exchange model are the regularized diagrams plotted in Fig. 1. Therefore it is not surprising that these models contradict the present understanding of nuclear structure. The fact that they reproduce the nucleon-nucleon data is no evidence of their validity because the data are fitted and are purely on-shell.

From SU(3) and SU(6) symmetry one can calculate the ratio of the $\rho$ and $\omega$ coupling constants. The exact symmetry leads to $g_\omega^2/g_\rho^2 = 9$ and $\kappa_\omega/\kappa_\rho = 1/5$ [11]. However, the values for the vector coupling obtained in conventional boson-exchange models are typically $g_\omega^2/g_\rho^2 = 20$ [4,5]. Such differences cannot be explained by the fact that the SU(3) and SU(6) symmetries are broken.

Furthermore the $(0^+, 0)$ [i.e., $(J^P, T)$ ] mesons are under discussion. The most likely candidate is a measured resonance with a mass of 975 MeV. A second resonance with a very large width has been observed, and it has been interpreted as a two-$\pi$ correlation with a mass of about 600 MeV [2]. It is remarkable, that the recent models need a meson with a mass of about 600 MeV. It turns out that the mass of this meson is unimportant for our model because the long-range scalar force is already given by the low meson scale.

Moreover from perturbative QCD (PQCD) it is known that the asymptotic behavior of the meson-nucleon form factors is $Q^{-4}$ [12] instead of $Q^{-2}$, as used in the monopole approximation. Because one integrates to infinite momentum transfer when calculating the two nucleon wave function, such discrepancies are important.

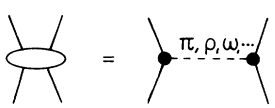


FIG. 1. Processes included in existing one-boson exchange models, where form factors are not calculated within the meson model, but are included as pure cut-offs. Therefore the form factors are artifacts of the potential model and two- or three- $\pi$ correlations have to be included as additional contributions.

 

## II. THE BOCHUM MODEL (RUHRPOT)

The Bochum approach to the $NN$ potential combines both meson degrees of freedom and the intrinsic nucleon structure at short distances [13]. By this we regard the interaction as a superposition of meson exchanges and direct $NN$ couplings, as shown in Fig. 2. The occurrence of such contact terms in the strong interaction is due to the inclusion of higher-mass mesons into the model. As the Lorentz structure $\mathcal{M}$ (shown in the Appendix) for one quantum-number exchange is unique, this leads, for example, in case of a $\rho$-like potential, to the following sum:

$$V_{\rho\text{-like}} = \mathcal{M}_{\rho\text{-like}}\left[\sum_{\beta} F^2_{NN\beta}(Q^2)\frac{g^2_{NN\beta}}{m^2_\beta + Q^2}\right] \quad (1)$$

$$= \mathcal{M}_{\rho\text{-like}}\left[F^2_{NN\rho}(Q^2)\frac{g^2_{NN\rho}}{m^2_\rho + Q^2} + \sum_{\beta\neq\rho} F^2_{NN\beta}(Q^2)\frac{g^2_{NN\beta}}{m^2_\beta + Q^2}\right], \quad (2)$$

$$= \mathcal{M}_{\rho\text{-like}}\left[F^2_{NN\rho}(Q^2)\frac{g^2_{NN\rho}}{m^2_\rho + Q^2} + F^2_{NN\rho\text{-direct}}(Q^2)\Sigma_{NN\rho}\right], \quad (3)$$

where $\beta$ stands for all $\rho$-like mesons. Because of the higher masses, the momentum dependence of the propagator for the additional mesons can be neglected, and one obtains an effective direct coupling as $\Sigma_{NN\rho}$ is an effective constant. As we will discuss later, the form factors dressing the contact interactions differ from those that dress the meson-nucleon vertex. The potential therefore takes the form

$$V = \left[V_{\text{meson}} + V_{\text{direct}}\right], \quad (4)$$

$$V_{\text{meson}} = \sum_{\alpha} \mathcal{M}_\alpha F^2_{NN\alpha}(Q^2)\frac{g^2_{NN\alpha}}{m^2_\alpha + Q^2}, \quad (5)$$

$$V_{\text{direct}} = \sum_{\alpha} \mathcal{M}_\alpha F^2_{NN\alpha\text{-direct}}(Q^2)\Sigma_{NN\alpha}, \quad (6)$$

with $\alpha = \pi, \rho, \omega, \delta, \epsilon, \eta$.

The meson sector is given by one-boson exchange processes and includes consistent vertex corrections which are calculated in the same framework in a one-loop ladder approximation [13,14]. We start from a renormalized Lagrangian with physical masses and pointlike particles, i.e., in the beginning the coupling constants $[F_{NN\alpha}(Q^2)g_{NN\alpha}]$ are momentum independent. We have used the densities shown in Table I plus the counterterms coming from the renormalization. The nucleon current is connected to the nucleon form factor for each meson $\alpha$ with the definition

$$\langle\psi_f|J_\alpha|\psi_i\rangle = \bar{u}(\mathbf{p}_f)\Gamma_{NN\alpha}u(\mathbf{p}_i)F_{NN\alpha}(Q^2). \quad (7)$$

We determine the extended structure of the nucleons by calculating the mesonic one-loop corrections to the nucleon current,

$$F_{NN\alpha}(Q^2) = 1 + \sum_i K^i_{NN\alpha}(Q^2) - (Z_{NN\alpha} - 1). \quad (8)$$

We calculate the contributing Feynman diagrams as shown in Fig. 3 and project out the operator structure $\bar{u}(\mathbf{p}_f)\Gamma_{NN\alpha}u(\mathbf{p}_i)$. Therefore the unity on the right-hand side of Eq. (8) is related to the tree graph of Fig. 3, i.e., the first diagram on the right-hand side of that figure. The different $K^i_{NN\alpha}$ are the different loop diagrams which contribute to the $NN\alpha$ vertex, and the index $i$ is introduced only to label them. The vertices are given by $H_I = -\int \mathcal{L}d^3x$. The last term of Eq. (8) is due to the renormalization and therefore connected to the counterterm $\Delta\mathcal{L} = (1 - Z_{NN\alpha})\bar{\psi}\Gamma_{NN\alpha}\psi$ which fixes the coupling constant to its physical value at $Q^2 = 0$. All loop diagrams of Eq. (8), i.e., Fig. 3, are divergent and have to be regularized. We replace the bare vertices with the self-consistent sum of one-loop diagrams as it is done in the Dyson equation, i.e., each bare vertex is replaced with the sum of all reducible higher-order diagrams. That leads to form factors on each meson-nucleon vertex in the loops as demonstrated in Fig. 4. In this scheme one has to distinguish two kinds of form factors. First we have to

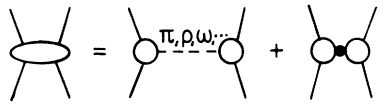


FIG. 2. The Bochum potential model includes (i) meson exchange and (ii) direct terms. Both the form factors and the $NN$ interaction are calculated within the same framework of the meson model, so that the nucleon structure is consistently taken into account and two- and three- $\pi$ correlations are included. All scales are consistent with the present understanding of the nuclear structure.

TABLE I. Lagrange densities of the present model (Ruhrpot).

| | $(J^P, T)$ | Lagrange densities |
|---|---|---|
| $\pi$ - like | $(0^-, 1)$ | $\frac{g}{2m_N}F_1(Q^2)\bar{\psi}\gamma^\mu\gamma^5\tau_i\psi\partial_\mu\phi_i$ |
| $\eta$ - like | $(0^-, 0)$ | $\frac{g}{2m_N}F_1(Q^2)\bar{\psi}\gamma^\mu\gamma^5\psi\partial_\mu\phi$ |
| $\rho$ - like | $(1^-, 1)$ | $-g\bar{\psi}\left[F_1(Q^2)\gamma_\mu - F_2(Q^2)\frac{\kappa}{2m_N}\sigma_{\mu\nu}\partial^\nu\right]\tau_i\psi\phi^\mu_i$ |
| $\omega$ - like | $(1^-, 0)$ | $-g\bar{\psi}\left[F_1(Q^2)\gamma_\mu - F_2(Q^2)\frac{\kappa}{2m_N}\sigma_{\mu\nu}\partial^\nu\right]\psi\phi^\mu$ |
| $\delta$ - like | $(0^+, 1)$ | $-gF_1(Q^2)\bar{\psi}\tau_i\psi\phi_i$ |
| $\epsilon$ - like | $(0^+, 0)$ | $-gF_1(Q^2)\bar{\psi}\psi\phi$ |

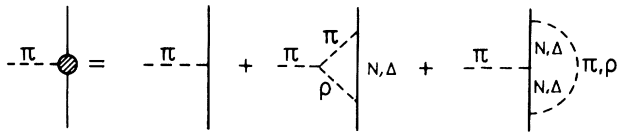


FIG. 3. Integral equation for calculating the one-loop corrections to the $NN\pi$ vertex. Note that similar equations have to be solved for all mesons, for example, the $NN\rho$ vertex is dominated by the $\pi\pi$ intermediate states. We have included the hadrons $\pi, \rho, \omega, \epsilon, N$, and $\Delta$.

include form factors coming from different mesons, e.g., the $NN\pi$ vertex depends on the $NN\rho$ vertex. Therefore we have to solve the equations for all the different nucleon-meson form factors simultaneously. Second, we have to include the form factor which is determined by the equation itself. We replace these vertices with a so-called test function. To regularize all diagrams even in lowest order we also replace the bare vertex of the tree graph (first diagram on the right-hand side of Fig. 3). This leads to the coupled set of equations, which are also shown in Fig. 5:

$$F_{NN\alpha}(Q^2) = G_{NN\alpha}(Q^2) + \sum_i K^i_{NN\alpha}(Q^2, G_{NN\alpha}, F_{NN(\beta\neq\alpha)}) + [1 - Z_{NN\alpha}(Q^2)]G_{NN\alpha}(Q^2). \quad (9)$$

We have used the following: $F_{NN\alpha}(Q^2)$, form factor for the $NN\alpha$ vertex which depends on the momentum transfer. $G_{NN\alpha}(Q^2)$, test function for the $NN\alpha$ vertex which depends on the momentum transfer. $K^i_{NN\alpha}(Q^2, G_{NN\alpha}, F_{NN(\beta\neq\alpha)})$, Feynman diagrams (with loop) which contribute to the $NN\alpha$ vertex. The diagrams depend on the momentum transfer, on the test function, and on the form factors of the other vertices. The operator structure $\bar{u}(\mathbf{p}_f)\Gamma_{NN\alpha}u(\mathbf{p}_i)$ is projected out. $Z_{NN\alpha}$, renormalization constant which sets the coupling constant to its physical value at $Q^2 = 0$.

Note that we have approximated the $N\Delta\alpha$ vertices to be the same as the $NN\alpha$ vertices.

These equations are solved by varying the different test functions $G_{NN\alpha}$ for all the mesons $\alpha$ until the loop

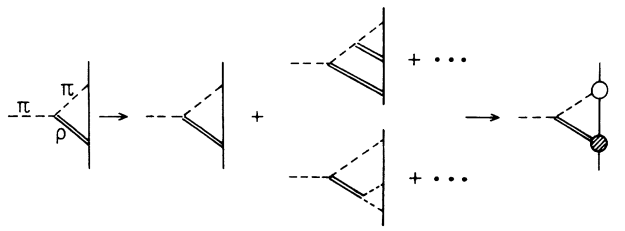


FIG. 4. Pictorial explanation of the self-consistent replacement of the bare vertices with dressed vertices. In step one the one-loop corrections are replaced with the sum of all reducible higher-order diagrams (ladder approximation). In the second step we identify the terms of the sum to be the form factors and the test function, respectively, so that all diagrams are regularized.

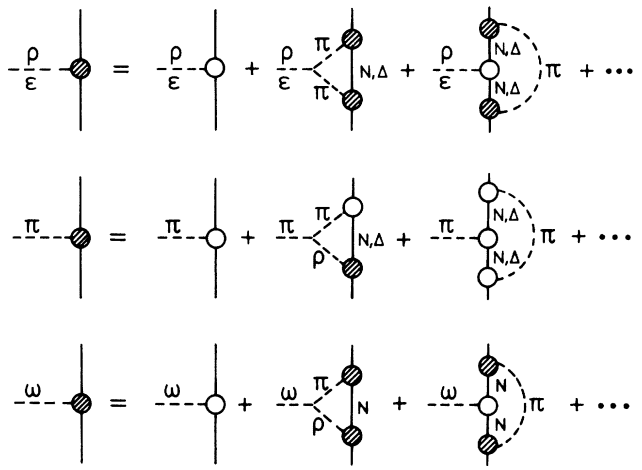


FIG. 5. Coupled set of integral equation which are explicitly solved. Note that we have approximated the $N\Delta$ form factors to behave like the related $NN$ form factors and that for the $\epsilon$ meson no $N, \Delta$ transition is possible.

corrections are momentum independent. Then, the test functions are equal to the form factors and the momentum independent loop contributions are absorbed in the renormalization constants. The same procedure is used to determine the Pauli form factor for the vector mesons. However, these form factors come purely from the mesonic one-loop corrections:

$$F_{2\ NN\alpha}(Q^2) = \frac{1}{g_{NN\alpha}} \sum_i K^i_{NN\alpha}(Q^2) \to \frac{1}{g_{NN\alpha}} \sum_i K^i_{NN\alpha}(Q^2, G_{NN\alpha}, F_{NN(\beta\neq\alpha)}). \quad (10)$$

To describe the nucleon structure for low $Q^2$ in a mathematically closed form, we have chosen a monopole form $F = \Lambda^2/(\Lambda^2 + Q^2)$. In Fig. 6 we show an exact cal-

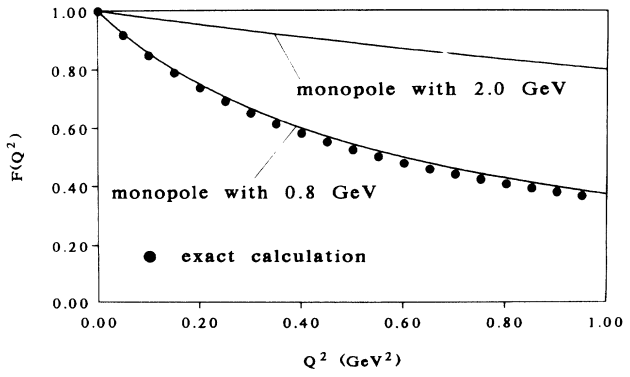


FIG. 6. Comparison of a self-consistent calculation of the one-$\pi$-loop contribution to the $NN\rho$ (Ref. [14]) compared to monopole form factors. The form factors of the present model are not adjusted with respect to the data, i.e., we have used a uniform scale of 0.8 GeV. The second curve is the form factor with a scale of $\lambda$=2.0 GeV, as obtained in the potential model Bonn B.

culation of the one-$\pi$-loop corrections to the $NN\rho$ form factor in comparison to the monopole representation with $\lambda = 0.8$ GeV. Note that the complete set of meson corrections are discussed in Refs. [13,14]. The complete calculation leads to meson scales between 0.6 and 0.9 GeV. However, the calculations have a principal uncertainty of about 100 MeV because not all coupling constants are determined. So, in the present model we have chosen a uniform scale for all vertices to demonstrate the possibility of reproducing the data without further adjustment of the form factors. We find that the form factors can be accurately represented by a monopole with a scale $\Lambda$ of 0.8 GeV except the $\epsilon$ meson $(0^+, 0)$, where we have chosen a scale $\Lambda = 0.64$ GeV. This exception results from the strong decay channel into two $\pi$ mesons. This is comparable to the $\rho$ meson, but in contrast to the $\epsilon$ meson, the $\rho$ meson form factor is strongly dominated by the magnetic term, especially by the $N\Delta\rho$ interaction [14].

By combining the one-boson-exchange diagrams with all contributing one-loop corrections to the vertices, all processes shown in Figs. 7 and 8 are taken into account. As the $\rho$, $\omega$, and $\epsilon$ mesons are correlated $\pi$ states, it is obvious that we have implicitly included the correlated two- and three-$\pi$ exchange processes. The two-$\pi$ states can be seen directly in Fig. 7 and the three-$\pi$ states can be seen in Figs. 8 and 9, where the $\omega$ decays as $\omega \to \rho\pi \to \pi\pi\pi$. Note that the integral equation for the vertex corrections in Fig. 5, just as the Schrödinger equation for the two nucleon wave function, iterates the included diagrams to infinite order, so that our description is not truncated to any finite order of coupling constants, but represents a topological class of diagrams, the so called ladder approximation.

To satisfy the asymptotic behavior of the strong interaction, we have extended the meson model. We adopt a phenomenological ansatz given by the analysis of the electromagnetic nucleon form factors by Gari and Krümpelmann [15], which is consistent with the present

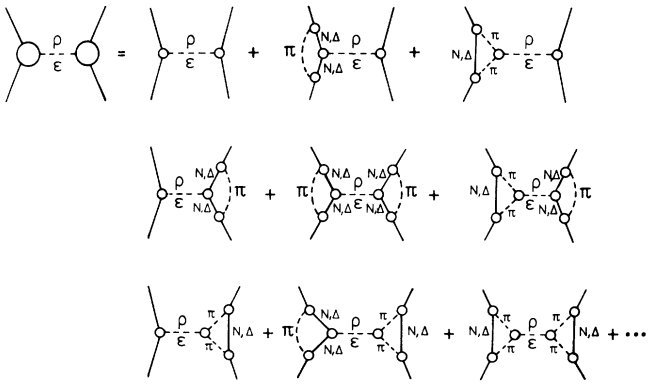

FIG. 7. Summary of most important processes which are actually included in the mesonic sector of the present Ruhrpot model, shown here for $\rho$- and $\epsilon$-meson exchanges. As the form factors are calculated within the same model they reflect consistently the nucleon structure arising from mesonic degrees of freedom. Two-$\pi$ correlations are included since the $\rho$ and $\epsilon$ mesons decay into $\pi\pi$. Note that for the $\epsilon$ meson no $N, \Delta$ transition is possible.

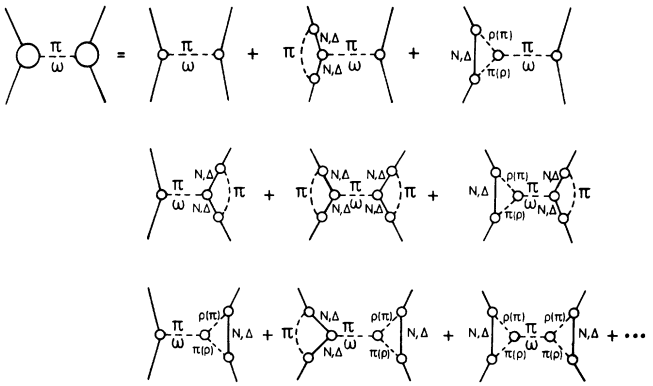

FIG. 8. Summary of most important processes which are actually included in the mesonic sector of the present Ruhrpot model, shown here for $\pi$- and $\omega$-meson exchanges. Three-$\pi$ correlations are included since the $\omega$ decay is dominated by $\omega \to \rho\pi \to \pi\pi\pi$. Note that for the $\omega$ meson no $N, \Delta$ transition is possible.

model of the strong interaction. Therefore the form factors are multiplied with additional monopole $(F_1)$ and dipole $(F_2)$ forms, respectively, both of which share the PQCD scale $\Lambda_2$:

$$F_{1,2}(Q^2) = \frac{\Lambda_1^2}{\Lambda_1^2 + \hat{Q}^2} \left[ \frac{\Lambda_2^2}{\Lambda_2^2 + \hat{Q}^2} \right]^{1,2}, \tag{11}$$

$$\hat{Q}^2 = Q^2 \frac{\log\left[\frac{\Lambda_2^2+Q^2}{\Lambda_{\rm QCD}^2}\right]}{\log\left[\frac{\Lambda_2^2}{\Lambda_{\rm QCD}^2}\right]},$$

$$\Lambda_1 = \begin{cases} 0.8 \text{ GeV} & \text{for mesons}, \\ 0.64 \text{ GeV} & \text{for the } (0^+, 0) \text{ meson}, \\ 1.2 \text{ GeV} & \text{for direct terms}, \end{cases}$$

$$\Lambda_2 = 2.3 \text{ GeV}, \quad \Lambda_{\rm QCD} = 0.29 \text{ GeV}.$$

The low-$Q^2$ behavior is essentially unchanged by the additional terms, but the asymptotic $Q^2$ dependence satisfies the counting rules of the PQCD [12]. The scale $\Lambda_2$ is fixed by the analysis of the electromagnetic form factors [15]. In this analysis the photon-nucleon coupling is described not only with an intermediate $\rho$ meson but also with a direct coupling itself. To be consistent with this very successful approach for the short-range part of the interaction, one has to investigate the direct coupling in the two-nucleon interaction as shown in Fig. 2. The

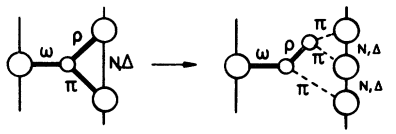

FIG. 9. Some of the three-$\pi$ states, which are included by our treatment of the meson vertices.

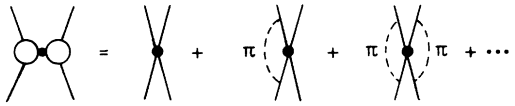


FIG. 10. Processes included in the long-range part of the direct terms of the present model.

long-range part of the direct vertices has to be calculated within the same framework as the meson corrections to the one-boson-exchange vertices. The contributing processes are shown in Fig. 10. As the decay channels of the high- and low-mass mesons are different, the important diagrams for the direct vertices are the loop diagrams where one meson is exchanged around a direct vertex. For example, in the $NN\rho$-like vertex we have to calculate the different kinds of loop diagrams, as shown in Fig. 11. The $\rho'$ meson cannot decay into two $\pi$ mesons and therefore the form factor is weaker and the range of the higher-mass mesons is shorter, as one would expect. Note that these diagrams are consistent with the effective Lagrangian introduced by Weinberg [17]. By summing up the long-range part of the diagrams within our model, that means the mesonic contributions to the direct terms, we obtain a form factor scale of 1.2 GeV for the direct terms. This is consistent with the analysis of the electromagnetic form factor [15]. The isovector part of that form factor is directly connected to the $\rho$-like strong form factors of the present model:

$$F_1^{iv}(Q^2) = \frac{g_\rho}{f_\rho}\frac{m_\rho^2}{m_\rho^2+Q^2}F_{1\ NN\rho}(Q^2) + \left[1-\frac{g_\rho}{f_\rho}\right]F_{1\ NN\rho\text{-direct}}(Q^2). \quad (12)$$

As mentioned before, the short-range part is parametrized due to the PQCD, and the results for the long-range part agree with the form factors used in the present model.

Comparing the meson exchanges and the direct terms one has two main effects. Due to the propagator, the meson-exchange contributions decrease with higher order in $Q^2$. As the form factor of the direct vertices has a weaker $Q^2$ dependence, this difference becomes even stronger. Therefore the meson exchange dominates the long-range part of the interaction and dies out at small distances. Thus the core is a property of the nucleonic structure only. We regard this distinction as the major step that is necessary to obtain good agreement with experiment without resorting to unrealistic and inconsistent scales, and we therefore regard this as one of the main advantages of our model.

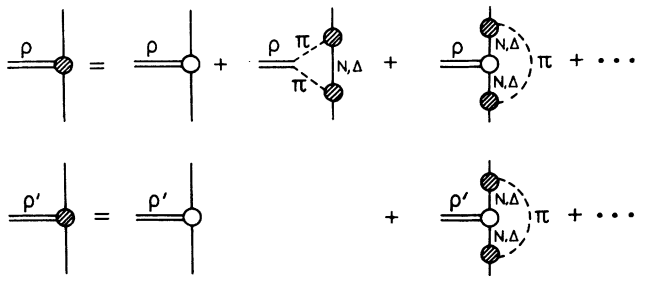


FIG. 11. Dominant contributions to the $NN\rho$-like form factors. For the higher-mass meson $\rho'$ the decay into two $\pi$ mesons is not possible.

## III. RESULTS AND DISCUSSION

The present model has some essential differences in comparison to conventional models.

(i) In the propagators, just as in the form factors, we take the four-momentum as it is obtained by summing up the time ordered diagrams in the perturbation expansion. Therefore it is possible to extend the model to a fully relativistic one [18].

(ii) Because the $(0^+,0)$ meson is still open to debate, we want to demonstrate that it is possible to use a meson with a mass of 975 MeV.

(iii) In the vector-meson sector we have restricted the coupling constants to be very close to the SU(3) and SU(6) values.

(iv) We have restricted the $NN\pi$ coupling constant because it has also come under scrutiny in the last years. de Swart and collaborators find, in their analysis of the $pp$ scattering data, a value for the uncharged $\pi$ of $g_\pi^2/4\pi = 13.5$ [19] . Note that this coupling is normalized at $Q^2 = m_\pi^2$, which is compatible with a value of about 13.1 at $Q^2 = 0$. Arndt *et al.* [20] obtain a value of 13.3 from their analysis of the $N\pi$ data. We restrict the $\pi$ coupling to be compatible with these results.

Some of the other coupling constants, i.e., the $\eta, \delta, \epsilon$, and the direct coupling constants, are completely unknown. Thus we have adjusted them to reproduce the $NN$ scattering data in terms of the phase shifts.

This procedure is nonetheless ambiguous because the phase shifts are not unique. Nowadays there are more than 4000 $NN$ scattering data available and usually they are represented via a phase shift analysis with more than 200 phase shifts. Because the experiments, and therefore also the phase shifts, are not independent it is meaningless simply to fit to these phase shifts. The Nijmegen group has shown that it is possible to reproduce the data ($\chi^2 < 1$) with a Reid-like parametrization with roughly 40 parameters [21]. Because the model is purely a phenomenological ansatz, it indicates a maximum number of the degrees of freedom in the data and shows that the phase shifts are strongly correlated. The only proper way to fit a potential is therefore to adjust the coupling constants with help of the so-called correlation matrix, which is the Hesse matrix of the phase shift analysis. This matrix contains all of the correlations between the phase shifts. We have used the analysis of the Nijmegen group [22] for the present results. The final assessment of the success of the potential model is, of course, the comparison with the data themselves, i.e., the calculated $\chi^2$ value to the data.

The analysis has included the $np$- and $pp$-scattering

TABLE II. Meson properties for the present model (Ruhrpot).

| Meson | $(J^P,T)$ | Mass | $g_i^2/4\pi$ | $\kappa_i$ | $\Sigma_i$ | $\kappa_i$ |
|---|---|---|---|---|---|---|
| $\pi$ | $(0^-,1)$ | 136.5 MeV | 13.288 | | 49.516 GeV$^{-2}$ | |
| $\eta$ | $(0^-,0)$ | 548.8 MeV | 2.8792 | | | |
| $\rho$ | $(1^-,1)$ | 776.0 MeV | 0.2169 | 6.4000 | 0.0124 GeV$^{-2}$ | 28.105 |
| $\omega$ | $(1^-,0)$ | 782.4 MeV | 1.9463 | 1.0880 | 12.379 GeV$^{-2}$ | 0.4334 |
| $\delta$ | $(0^+,1)$ | 983.0 MeV | 2.9059 | | | |
| $\epsilon$ | $(0^+,0)$ | 975.0 MeV | 8.8853 | | 5.6911 GeV$^{-2}$ | |

TABLE III. Phase shifts calculated with the present model (Ruhrpot). A complete set of phase shifts is included in the SAID program [23].

| | 10 MeV | 25 MeV | 50 MeV | 100 MeV | 200 MeV | 300 MeV |
|---|---|---|---|---|---|---|
| $^1S_0$ | 59.224 | 49.658 | 38.448 | 23.060 | 2.922 | -11.152 |
| $^3P_0$ | 3.989 | 8.527 | 10.851 | 8.368 | -1.209 | -10.064 |
| $^1P_1$ | -3.347 | -7.021 | -10.800 | -15.842 | -23.349 | -29.203 |
| $^3P_1$ | -2.329 | -5.334 | -8.737 | -13.336 | -20.248 | -26.171 |
| $^3S_1$ | 102.690 | 80.786 | 63.017 | 43.595 | 21.789 | 7.568 |
| $^3D_1$ | -0.720 | -2.938 | -6.671 | -12.541 | -20.249 | -25.608 |
| $E_1$ | 1.110 | 1.647 | 1.899 | 2.342 | 3.729 | 5.218 |
| $^1D_2$ | 0.177 | 0.700 | 1.652 | 3.666 | 7.319 | 9.423 |
| $^3D_2$ | 0.899 | 3.846 | 8.998 | 16.612 | 23.094 | 24.101 |
| $^3P_2$ | 0.668 | 2.463 | 5.784 | 11.087 | 15.690 | 16.216 |
| $^3F_2$ | 0.014 | 0.107 | 0.325 | 0.684 | 0.784 | 0.055 |
| $E_2$ | -0.218 | -0.843 | -1.720 | -2.515 | -2.247 | -1.453 |

TABLE IV. Low energy scattering parameters calculated with our $L = 0$ phase shifts.

| Spin | Observable | Theory | Experiment |
|---|---|---|---|
| $S = 0$ | Scattering length $a_s$ | -23.80 fm | -23.748(10) fm |
| | Effective range $r_s$ | 2.75 fm | 2.75(5) fm |
| $S = 1$ | Scattering length $a_t$ | 5.42 fm | 5.419(10) fm |
| | Effective range $r_t$ | 1.75 fm | 1.754(8) fm |

TABLE V. Deuteron properties as obtained from the present model (Ruhrpot).

| Observable | | Theory | Experiment |
|---|---|---|---|
| Deuteron binding energy | $E_D$ | -2.224 MeV | -2.224575(9) MeV |
| $D$-wave probability | $P_D$ | 5.85 % | — |
| Quadrupole moment | $Q_D$ | 0.276 fm$^2$ | 0.2860(15) fm$^2$ |
| | | | 0.2859(3) fm$^2$ |
| Asymptotic | $A_S$ | 0.882 fm$^{-\frac{1}{2}}$ | 0.8846(8) fm$^{-\frac{1}{2}}$ |
| Asymptotic | $D/S$ | 0.025 | 0.0271(8) |
| | | | 0.0272(4) |
| | | | 0.0256(4) |
| Root mean square radius | $r_D$ | 1.932 fm | 1.9635(45) fm |
| | | | 1.9560(68) fm |
| | | | 1.953(3) fm |

data. Due to the Coulomb force in the $pp$ system these two data sets have different $^1S_0$ phases. As we have not included any Coulomb interactions, we have used only the $^1S_0$ phases of the $np$ system, so our model gives good results for all $np$ experiments and for $pp$ experiments above 10 MeV, where the Coulomb force becomes negligible.

We have solved the Lippmann-Schwinger equation to calculate the phase shifts and obtained the set of coupling constants shown in Table II. In Table III we list the phases for $J \leq 2$. A complete set of our phases is included in the SAID program under the name RUHR [23]. Table IV contains the low energy scattering parameters that are calculated with our $L = 0$ phase shifts.

To calculate the deuteron observables, we have solved the Schrödinger equation. We have calculated a number of deuteron properties in impulse approximation and the results are presented in Table V. For detailed information about the experimental values quoted we refer to [13] and the references therein. Note that the coupling constants are determined purely by the fit to the phase shifts, whereas the low energy parameters and the deuteron properties are calculated without further adjustment of the coupling constants, as they reproduce the experiments already. In particular, the deuteron binding energy is not used to adjust the parameters. Comparing the theoretical deuteron properties such as quadrupole moment, root mean square radius, and asymptotic behavior with experiment one recognizes that the data are underestimated. This probably results from neglecting the photon coupling to meson exchange-currents, which are not taken into account via an impulse approximation. As already mentioned the most important criteria of the potential models are the direct comparison with the $NN$ scattering data rather, than simply the phase shifts. We have calculated them with the SAID program [23] and the $\chi^2$ values for $np$ scattering up to 300 MeV are presented in Table VI for comparison with other realistic potential models, all of which are presently included in the SAID program. Although it is demonstrated by the Nijmegen group that it is possible to find a parameterization which produces a $\chi^2$ value below 1, our model shows a reasonable agreement with the data compared to other meson-exchange models. Note that such data fix only the on-shell behavior of the models. Therefore it is extremely important to investigate and measure the off-shell behavior in experiments like $(p, p\gamma)$ bremsstrahlung or elastic and inelastic deuteron electron scattering [25].

Summarizing our results, we note that a consistent microscopic meson-exchange model at low $Q^2$ with a realistic and consistent extension to high $Q^2$ is a valuable tool to describe the nucleon-nucleon interaction. In the mesonic sector we have included not only the pure meson exchanges, but also the vertex corrections calculated within the same model. Therefore we have also included the two- and three-$\pi$ correlations in a consistent manner. We obtained a meson scale of 0.8 GeV for the meson-exchange vertices and 1.2 GeV for the direct vertices from both the mesonic calculation and the analysis of the electromagnetic form factor. The PQCD scale $\Lambda_2$ in this model is taken from an analysis of the electromagnetic form factor. Due to the weaker form factor and the missing $Q^2$ dependence of the propagator of the direct interactions, meson-exchange processes become unimportant at small distances and the core is dominated by the nucleonic structure. We have demonstrated that such a model gives a good description of the available data and that inconsistencies appearing in most existing meson-exchange models are indeed avoidable.

TABLE VI. Comparison of several realistic potential models. The $\chi^2$'s are obtained by comparison with all measured observables in np scattering up to 300 MeV. For detailed information on these models we refer to the references given in the SAID program [23]. Note that the updated Nijmegen potential gives a $\chi^2$ of 2.1 to their $np$ data.[a]

| Model | $\chi^2$ |
|---|---|
| Bonn (full) | 1.82 |
| Bonn B (OBE) | 2.27 |
| Nijmegen (92) | 4.41 (2.1) |
| Paris (81) | 4.16 |
| Ruhrpot (this work) | 1.68 |

[a]The differences resulting from the Nijmegen groups treatment of some total cross section data [24].

## ACKNOWLEDGMENTS

We wish to acknowledge help of the Nijmegen group, especially J. J. de Swart and Vincent Stoks who provided us with their most recent phase shift analysis and the correlation matrix before publication. We also acknowledge Dick Arndt for his considerable help on the $NN$ data. This work was supported by COSY-KFA Jülich (41140512) and Deutsche Forschungsgemeinschaft (Ga 153/11-4).

## APPENDIX: EXPLICIT POTENTIAL STRUCTURE

In time-ordered perturbation theory, an effective one-boson exchange potential is given by

$$V_{\text{eff}} = \frac{1}{2} \sum_{\alpha} H_I^{\alpha} \left\{ \frac{1}{\epsilon_i - H_0} + \frac{1}{\epsilon_f - H_0} \right\} H_I^{\alpha}, \qquad \text{(A1)}$$

where $\epsilon_i$ and $\epsilon_f$ are the asymptotic energies of the initial and the final states, $H_0$ is the free energy operator, and $H_I^{\alpha}$ is the interaction energy obtained from integrating the Lagrange densities presented in Table I via $H_I = -\int \mathcal{L} d^3x$. Note that, in principle, one has to sum over all mesons $\alpha$. In our approach, where we take the lightest mesons exactly into account, and the higher mass effects via direct terms, the potential becomes

$$V_{\rm eff} = \frac{1}{2}\left[\sum_{\alpha_1} H_I^{\alpha_1}\left\{\frac{1}{\epsilon_i - H_0} + \frac{1}{\epsilon_f - H_0}\right\} H_I^{\alpha_1} + \sum_{\alpha_2} H_I^{\alpha_2}\Sigma_{\alpha_2} H_I^{\alpha_2}\right]. \tag{A2}$$

Including all elements explicitly one obtains the final potential structure for each meson, which can be defined in terms of the Lorentz structure $\mathcal{M}$ of the vertices and the propagators times some constants:

$$\begin{aligned} V_{\left\{\substack{is\\iv}\right\}}(\mathbf{p},\mathbf{p}') &= \sum_\alpha \left[\frac{g_{NN\alpha}^2}{m_\alpha^2 - k_\mu^2}\right] F_{NN\alpha}^2(k^2)\mathcal{M}_\alpha \\ &= \sum_\alpha \left[\frac{g_{NN\alpha}^2}{4\pi}\frac{1}{m_\alpha^2 - k_\mu^2}\right]\frac{1}{8\pi^2}\frac{e_p e_{p'}}{E_p E_{p'}}\begin{Bmatrix}\mathbb{1}\\ \boldsymbol{\tau}_1\cdot\boldsymbol{\tau}_2\end{Bmatrix} \\ &\quad \times V_0^\alpha \mathbb{1} + V_1^\alpha i\mathbf{S}(\mathbf{k}\times\mathbf{q}) + V_2^\alpha(\boldsymbol{\sigma}_1\cdot\mathbf{k})(\boldsymbol{\sigma}_2\cdot\mathbf{k}) + V_3^\alpha(\boldsymbol{\sigma}_1\cdot\mathbf{q})(\boldsymbol{\sigma}_2\cdot\mathbf{q}) \\ &\quad + V_4^\alpha[\boldsymbol{\sigma}_1\cdot(\mathbf{k}\times\mathbf{q})][\boldsymbol{\sigma}_2(\mathbf{k}\times\mathbf{q})] + V_5^\alpha(\boldsymbol{\sigma}_1\cdot\boldsymbol{\sigma}_2), \end{aligned} \tag{A3}$$

where

$$k_\mu = p_\mu - p'_\mu, \quad q_\mu = (p_\mu + p'_\mu)/2, \quad \mathbf{S} = (\boldsymbol{\sigma}_1 + \boldsymbol{\sigma}_2)/2,$$

and

$$e_p = E_p + m = \sqrt{\mathbf{p}^2 + m^2} + m.$$

1. Pseudoscalar exchange; isoscalar $(is)(0^-,0)$ and isovector $(iv)(0^-,1)$ (A4)

$$\begin{aligned} V_2 &= F^2(k_\mu^2)\left[-\frac{1}{4}\frac{(e_p+e_{p'})^2}{e_p^2 e_{p'}^2} + \frac{\mathbf{q}^2}{e_p^2 e_{p'}^2}\frac{e_p+e_{p'}}{E_p+E_{p'}}\right], \\ V_3 &= F^2(k_\mu^2)\left[-\frac{(E_p-E_{p'})^2}{e_p^2 e_{p'}^2} + \frac{\mathbf{k}^2}{e_p^2 e_{p'}^2}\frac{e_p+e_{p'}}{E_p+E_{p'}}\right], \\ V_4 &= F^2(k_\mu^2)\left[\frac{1}{e_p^2 e_{p'}^2}\frac{e_p+e_{p'}}{E_p+E_{p'}}\right], \\ V_5 &= F^2(k_\mu^2)\left[-\frac{(\mathbf{k}\times\mathbf{q})^2}{e_p^2 e_{p'}^2}\frac{e_p+e_{p'}}{E_p+E_{p'}}\right]. \end{aligned}$$

2. Scalar exchange; isoscalar $(is)(0^+,0)$ and isovector $(iv)(0^+,1)$ (A5)

$$\begin{aligned} V_0 &= F^2(k_\mu^2)\left[-\left(1 - \frac{\mathbf{p}'\cdot\mathbf{p}}{e_p e_{p'}}\right)^2\right], \\ V_1 &= F^2(k_\mu^2)\left[\frac{2}{e_p e_{p'}}\left(\frac{\mathbf{p}'\cdot\mathbf{p}}{e_p e_{p'}} - 1\right)\right], \\ V_4 &= F^2(k_\mu^2)\left[\left(\frac{1}{e_p e_{p'}}\right)^2\right]. \end{aligned}$$

3. Vector exchange; isoscalar $(is)(1^-,0)$ and isovector $(iv)(1^-,1)$ (A6)

$$\begin{aligned} V_0 &= [F_1(k_\mu^2) + \kappa F_2(k_\mu^2)]^2\left[\left(\frac{\mathbf{p}'}{e_{p'}} + \frac{\mathbf{p}}{e_p}\right)^2 + \left(1 + \frac{\mathbf{p}'\cdot\mathbf{p}}{e_p e_{p'}}\right)^2\right] \\ &\quad - \frac{[F_1(k_\mu^2) + \kappa F_2(k_\mu^2)]\kappa F_2(k_\mu^2)}{m}\left[\frac{\mathbf{p}'\cdot\mathbf{p}}{e_{p'}}\left(1 - \frac{\mathbf{p}'^2}{e_p e_{p'}} - \frac{\mathbf{p}'\cdot\mathbf{p}}{e_p e_{p'}}\right) + \frac{\mathbf{p}'^2}{e_{p'}}\right. \\ &\quad \left. + \frac{\mathbf{p}^2}{e_p} + \frac{\mathbf{p}'\cdot\mathbf{p}}{e_p}\left(1 - \frac{\mathbf{p}^2}{e_p e_{p'}} - \frac{\mathbf{p}'\cdot\mathbf{p}}{e_p e_{p'}}\right) + (E_p + E_{p'})\left(1 - \frac{(\mathbf{p}'\cdot\mathbf{p})^2}{e_p^2 e_{p'}^2}\right)\right] \\ &\quad + \left(\frac{\kappa F_2(k_\mu^2)}{m}\right)^2\left[\left(1 - \frac{\mathbf{p}'\cdot\mathbf{p}}{e_p e_{p'}}\right)^2\left(\mathbf{q}^2 + \frac{1}{4}(E_p + E_{p'})^2\right)\right], \\ V_1 &= [F_1(k_\mu^2) + \kappa F_2(k_\mu^2)]^2\left[-\frac{6}{e_p e_{p'}} - 2\frac{\mathbf{p}'\cdot\mathbf{p}}{e_p^2 e_{p'}^2}\right] + \frac{[F_1(k_\mu^2) + \kappa F_2(k_\mu^2)]\kappa F_2(k_\mu^2)}{m}\left[\frac{1}{e_{p'}}\left(1 - \frac{\mathbf{p}'^2}{e_p e_{p'}} - 2\frac{\mathbf{p}'\cdot\mathbf{p}}{e_p e_{p'}}\right)\right. \\ &\quad \left. + \frac{1}{e_p}\left(1 - \frac{\mathbf{p}^2}{e_p e_{p'}} - 2\frac{\mathbf{p}'\cdot\mathbf{p}}{e_p e_{p'}}\right) - 2(E_p + E_{p'})\frac{\mathbf{p}'\cdot\mathbf{p}}{e_p^2 e_{p'}^2}\right] \\ &\quad + \left(\frac{\kappa F_2(k_\mu^2)}{m}\right)^2\left[2\left(\frac{1}{e_p e_{p'}} - \frac{\mathbf{p}'\cdot\mathbf{p}}{e_p^2 e_{p'}^2}\right)\left(\mathbf{q}^2 + \frac{1}{4}(E_p + E_{p'})^2\right)\right], \end{aligned}$$

$$V_2 = [F_1(k_\mu^2) + \kappa F_2(k_\mu^2)]^2 \left[\frac{1}{4}\left(\frac{1}{e_p} + \frac{1}{e_{p'}}\right)^2 - \frac{\mathbf{q}^2}{e_p^2 e_{p'}^2}\frac{e_p + e_{p'}}{E_p + E_{p'}}\right],$$

$$V_3 = [F_1(k_\mu^2) + \kappa F_2(k_\mu^2)]^2 \left[\left(\frac{1}{e_p} - \frac{1}{e_{p'}}\right)^2 - \frac{\mathbf{k}^2}{e_p^2 e_{p'}^2}\frac{e_p + e_{p'}}{E_p + E_{p'}}\right],$$

$$V_4 = [F_1(k_\mu^2) + \kappa F_2(k_\mu^2)]^2 \left[-\frac{E_p + E_{p'} + e_p + e_{p'}}{(E_p + E_{p'})e_p^2 e_{p'}^2}\right] + \frac{[F_1(k_\mu^2) + \kappa F_2(k_\mu^2)]\kappa F_2(k_\mu^2)}{m}\left[-\frac{E_p + E_{p'} + e_p + e_{p'}}{e_p^2 e_{p'}^2}\right]$$
$$+ \left(\frac{\kappa F_2(k_\mu^2)}{m}\right)^2 \left[-\frac{\mathbf{q}^2 + [(E_p + E_{p'})/2]^2}{e_p^2 e_{p'}^2}\right],$$

$$V_5 = [F_1(k_\mu^2) + \kappa F_2(k_\mu^2)]^2 \left[-\left(\frac{\mathbf{p}'}{e_{p'}} - \frac{\mathbf{p}}{e_p}\right)^2 + \frac{(\mathbf{k}\times\mathbf{q})^2}{e_p^2 e_{p'}^2}\frac{e_p + e_{p'}}{E_p + E_{p'}}\right].$$

The potential structure for the direct interactions can be obtained by the substitution

$$\left[\frac{g^2}{4\pi}\frac{1}{m^2 - k_\mu^2}\right] \quad \text{with} \quad [\Sigma], \tag{A7}$$

and the meson-scale form factors should be replaced by their direct counterparts.


[1] R. V. Reid, Ann. Phys. (N.Y.) **50**, 411 (1968); A. D. Jackson, D. O. Riska, and B. VerWest, Nucl. Phys. **A249**, 397 (1975); F. Partovi and E. L. Lomon, Phys. Rev. D **14**, 2402 (1976); G. E. Brown and A. D. Jackson, *The Nucleon-Nucleon Interaction* (North-Holland, Amsterdam, 1976); I. E. Lagaris and V. R. Pandharipande, Nucl. Phys. **A359** 331 (1981); R. B. Wiringa, R. A. Smith, and T. L. Ainsworth, Phys. Rev. C **29**, 1207 (1984).

[2] J. J. de Swart, W. A. van der Sanden, and W. Derks, Nucl. Phys. **A416**, 299c (1984).

[3] M. Lacombe, B. Loiseau, J. M. Richard, R. Vin Mau, J. Côté, P. Pirès, and R. de Tourreil, Phys. Rev. C **21**, 861 (1980).

[4] R. Machleidt, K. Holinde, and Ch. Elster, Phys. Rep. **149**, 1 (1987).

[5] F. Gross, J. W. Van Orden, and K. Holinde, Phys. Rev. C **41**, R1909 (1990).

[6] T. D. Cohen, Phys. Rev. D **34**, 2187 (1986); N. Kaiser, U. G. Meissner, and W. Weise, Phys. Lett. B **198**, 319 (1987).

[7] P. Alberto, E. Ruiz Arriola, M. Fiolhais, F. Grümmer, J. N. Urbano, and K. Goeke, Phys. Lett. B **208**, 75 (1988).

[8] A. W. Thomas and K. Holinde, Phys. Rev. Lett. **63**, 2025 (1989).

[9] B. L. G. Bakker, M. Brozoian, J. N. Maslow, and H. J. Weber, Phys. Rev. C **25**, 1134 (1982).

[10] J. V. Noble, Phys. Rev. Lett. **46**, 412 (1981); Chr. V. Christov, E. Ruiz Arriola, and K. Goeke, Nucl. Phys. **A510**, 689 (1990).

[11] J. J. de Swart, Rev. Mod. Phys. **35**, 916 (1963); M. M. Nagels, T. A. Rijken, and J. J. de Swart, Ann. Phys. (N.Y.) **79**, 338 (1973).

[12] S. J. Brodsky and G. P. Lepage, Phys. Rev. D **22**, 2157 (1980).

[13] S. Deister, M. F. Gari, W. Krümpelmann, and M. Mahlke, Few-Body Syst. **10**, 1 (1991).

[14] J. Flender and M. F. Gari, Z. Phys. A **343**, 467 (1992); and (unpublished).

[15] M. F. Gari and W. Krümpelmann, Phys. Lett. B **173**, 10 (1986); Phys. Rev. D **45**, 1817 (1992); **46**, 484 (1992).

[16] S. Théberge, A. W. Thomas, and G. A. Miller, Phys. Rev. D **22**, 2838 (1980).

[17] S. Weinberg, Phys. Lett. B **251**, 288 (1990).

[18] D. Plümper and M. F. Gari, Z. Phys. A **343**, 343 (1992).

[19] V. G. J. Stoks, R. Timmermans, and J. J. de Swart, Phys. Rev. C **47**, 512 (1993).

[20] R. A. Arndt, Z. Li, L. D. Roper, and R. L. Workman, Phys. Rev. Lett. **65**, 157 (1990); R. A. Arndt and R. L. Workman, Phys. Rev. C **43**, 2436 (1991).

[21] V. G. J. Stoks and J. J. de Swart, Phys. Rev. C **47**, 761 (1993).

[22] V. G. J. Stoks, R. A. M. Klomp, M. C. M. Rentmeester, and J. J. de Swart, Phys. Rev. C **48**, 792 (1993).

[23] R. A. Arndt, L. D. Roper, R. L. Workman, and M. W. McNaughton, Phys. Rev. D **45**, 3995 (1992).

[24] V. G. J. Stoks (private communication).

[25] J. Eden, D. Plümper, M. F. Gari, and H. Hebach, Z. Phys. A **347**, 145 (1994).